RSC Advances

PAPER

View Article Online
View Journal | View Issue

Cite this: *RSC Adv.*, 2023, **13**, 3164

Structural and photoelectron spectroscopic study on the heterotrinuclear nickel–titanium dioxide carbonyl complexes $Ni_2TiO_2(CO)_n^-$ ($n = 2–4$)†

Shihu Du,[ad] Haiyan Han,*[a] Yongliang Yan,[b] Yantao Lv,[b] Zhihui Fan,[a] Xiuhong Liu,[a] Xiaoqing Liang,[c] Hua Xie,[d] Zhi Zhao*[a] and Ruili Shi*[a]

Received 12th December 2022
Accepted 12th January 2023

DOI: 10.1039/d2ra07918f

rsc.li/rsc-advances

Herein, the configurations and intrinsic electronic properties of heteronuclear transition metal dioxide carbonyl anions $Ni_2TiO_2(CO)_n^-$ ($n = 2–4$) in the gas phase were investigated using mass spectrometry coupled anionic photoelectron spectroscopy, *ab initio* calculations, and simulated density-of-state (DOS) spectra. The results clearly show that the binding of electrons is enhanced by the addition of CO. The ground state structures of $Ni_2TiO_2(CO)_n^-$ ($n = 2–4$) are characterized to show that three transition metal atoms (one Ti atom and two Ni atoms) forming a quasi-line is favored. The interaction between Ni and C becomes weaker as the cluster size increases. The natural electron configuration shows that the extra electron is enriched on O atoms attached to Ti, and there is strong interaction between Ti and O atoms. This work gives significant insight into the configuration and electronic structures of nickel-titanium dioxide carbonyl anions, which has potential application in adsorption of carbon monoxide on the surfaces/interfaces of alloys.

1. Introduction

The interaction between carbon monoxide (CO) and transition metal (TM) containing metal compounds, and oxide complexes attracts lots of attention due to its great significance in catalytic chemistry, coordination chemistry, medicine, and material science.[1–4] Transition metal carbonyls or transition metal oxide carbonyls could provide well-defined models of CO adsorption on the surfaces/interfaces of alloys or the binding at active sites of catalysts.[5,6] For muti adsorption of carbon monoxide on a transition metal (oxide), great effort has been made to search the ground state structures both in experiment and theory.[7–9] The CO molecules usually adsorb to the transition metal atoms to form side-on-bonded, bridging, or terminal modes.[10,11] Meanwhile, the maximum carbonyl-coordination number of mononuclear metal has been extensively studied.[12–16] The multinuclear transition metal carbonyl compounds have also gained increasing interest in the last few years.[17–30]

Subsequently, the study on the reaction of metal oxide clusters with CO also gradually enriched. For the metal oxide carbonyls, the $MO(CO)_5^+$ (M = Sc, Y, La and Ce) is similar to a pentagonal pyramidal structure with C_{5V} symmetry.[31] The maximum carbonyl-coordination number of $ScO(CO)_n^+$, $YO(CO)_n^+$ and $LaO(CO)_n^+$ is 6, 7 and 9, respectively.[32–34] On the side of heterobinuclear transition metal oxide carbonyls, the sequential adsorption of CO in $NbNiO(CO)_{5–8}^-$ and $TaNiO(CO)_{4–8}^-$ clusters can promote the competitive binding with oxygen atom to the transition metal centers.[35,36] Many researches focus on the oxidation of CO when studying the interaction between CO and transition metal oxide (TMO) since CO oxidation is one of the most important prototypical reactions.[35–39] The TM atom acts as a preferred trapping site for CO adsorption and accepts the electron from CO. Then the ligand CO could be oxidized by the oxygen species on the TMO cluster. Moreover, the CO could directly react with the oxygen atom in TMO.[36] For heteronuclear TMO, experimental observations combined with quantum chemistry calculations confirm that there is oxidation of CO in $ScOFe(CO)_5^-$, $YOFe(CO)_5^-$,[40] $NbNiO(CO)_{7–8}^-$,[35] $Ni_2VO_{4,5}CO^-$,[41] and $TaNiO(CO)_8^-$ complexes.[36] While there is no oxidation of CO in $LaOFe(CO)_5^-$ anion.[40] Therefore, different ratios and types of TMO will affect the results of CO oxidation reaction.

[a]*School of Mathematics and Physics Science and Engineering, Hebei University of Engineering, Handan 056038, China. E-mail: hanhy0226@163.com; zhaozhi@hebeu.edu.cn; shiruili@hebeu.edu.cn*

[b]*School of Information and Electrical Engineering, Hebei University of Engineering, Handan 056038, China*

[c]*Department of Physics, Taizhou University, Taizhou 318000, China*

[d]*State Key Laboratory of Molecular Reaction Dynamics, Dalian Institute of Chemical Physics, Chinese Academy of Sciences, Dalian 116023, China*

† Electronic supplementary information (ESI) available: The total energies of several anion/neutral isomers of $Ni_2TiO_2(CO)_n^{-1/0}$ ($n = 2–4$) clusters with different spin multiplicities. The structures, relative energies, and symmetries of the isomers with higher energies of $Ni_2TiO_2(CO)_n^-$ ($n = 3, 4$) clusters. Experimental and theoretical VDEs and ADEs as well as theoretical relative energies of the higher energy structures of $Ni_2TiO_2(CO)_n^-$ ($n = 3, 4$) clusters. Cartesian coordinates of all carbonyl isomers of $Ni_2TiO_2(CO)_n^-$ ($n = 2–4$). See DOI: https://doi.org/10.1039/d2ra07918f

The above-mentioned researches rarely involve the interaction between CO and heteronuclear transition metal dioxide. The geometry, electronic structures, and the containing of CO oxidation for the heteronuclear transition metal dioxide carbonyl complexes are unclear. In this work, using experimental PES and theoretical investigation, we report the structures and electronic properties of the heteronuclear transition metal dioxide carbonyl anions $Ni_2TiO_2(CO)_n^-$ (n = 2–4) in gas phase. The anions are produced *via* a laser vaporization supersonic cluster source, selected by a dual channel mass spectrometer (D-TOFMS), and then analyzed using a velocity-map imaging spectrometer. Meanwhile, the structures, energetic and electronic properties are performed by *ab initio* calculations to further understand the experimental observation. The consistency of experimental and simulated results reveals that the three transition metal atoms form a quasi-line and there is no oxidation of CO in $Ni_2TiO_2(CO)_n^-$ (n = 2–4) clusters.

2. Experimental and theoretical methods

2.1. Experiment

The photoelectron detachment experiments were carried out with a homemade device which included a laser vaporization source, a D-TOFMS and a velocity-map imaging spectrometer. A detailed description of the instrument has already been provided elsewhere,[42] so what follows is merely an outline. $Ni_2TiO_2(CO)_n^-$ (n = 2–4) clusters were fabricated by ablating a small Ti/Ni target (mole ratio, Ti/Ni = 1 : 1) with a laser vaporization (532 nm) beam in the presence of helium carrier gas seeded with 5% CO. Stagnation of the carrier gas was approximately 4 atm. Cluster anions expanded into the source chamber after being cooled. Wiley–McLaren time-of-flight mass spectrometer was used to mass select these anionic clusters. For the detachment of these anionic clusters, photon energy of 355 nm (3.496 eV) was employed. The photoelectrons were mapped onto a detector consisting of a micro-channel plate and a phosphor screen. The two-dimensional (2D) images on the phosphor screen were recorded by a charge-coupled-device (CCD) camera. Each image was obtained by accumulating 10 000–50 000 laser shots at 10 Hz repetition rate. All of the raw images were reconstructed using the basis set expansion inverse Abel transform method (BASEX). The photoelectron spectra were calibrated using the known spectrum of Au^-.[43–45] The PES were plotted against electron binding energy eBE = $h\nu$ − eKE, where $h\nu$ is the photon energy. The typical energy resolution was about 50 meV full width at half maximum (FWHM) at electron kinetic energy (eKE) of 1 eV.

2.2. Theory

We used BP86 functional, which has been verified to be outstanding for describing the transition metal carbonyl compounds in the previous works,[35,46] and ma-TZVP basis set to elucidate the geometrical, energetic, and electronic properties of $Ni_2TiO_2(CO)_n^-$ (n = 2–4) clusters. The BP86 functional combines Becke's 1988 exchange functional (B)[47] with Perdew's 1986 gradient corrected correlation functional method (P86).[48] The ma-TZVP basis set is a modification of the standard def2-TZVP basis set[49] with diffuse functions for atoms heavier than He by dividing the smallest s and p exponential parameters already present by a factor of 3.[50,51] Meanwhile, many possible spin multiplicities were considered, including doublets, quartet and sextet for $Ni_2TiO_2(CO)_n^-$, and singlet, triplet and quintet for neutral $Ni_2TiO_2(CO)_n$, respectively. The results are shown in Tables S1 and S2 of the ESI.† The lowest spin state, *i.e.* doublets for $Ni_2TiO_2(CO)_n^-$ and singlets for $Ni_2TiO_2(CO)_n$ are most stable. The structures were fully optimized without any symmetry constraint. Frequency analyses at the same level of theory with geometry optimizations were performed to confirm that each optimized structure is a true minimum on potential energy surface without imaginary frequency. The zero-point-energy (ZPE) corrections were considered in the total energy of each cluster isomer for relative energy and adiabatic detachment energy (ADE) calculations.

The simulated photoelectron spectrum for a given isomer is based on the generalized Koopmans' theorem.[52–55] The vertical detachment energy (VDE) was calculated as the difference in energy between the neutral and anionic species based on the optimized anionic geometry. The ADE was calculated as the difference in energy between the neutral and the anion both at the related optimized configurations. The calculated density of states was then globally shifted in order to align the binding energies of the HOMO with the theoretical VDE value.[56,57] In order to better understand the electronic structure of the $Ni_2TiO_2(CO)_n^-$ clusters, we calculated the natural electron configuration using natural bond orbital (NBO) analyses. All of the calculations were carried out with the Gaussian09 package.[58]

3. Results and discussion

3.1. Photoelectron spectra in experiment

The photoelectron images and the corresponding photoelectron spectra of $Ni_2TiO_2(CO)_n^-$ (n = 2–4) recorded at 355 nm are shown in Fig. 1. Note that the experimental error bars are determined by our instrumental resolution. The main band in the spectrum of $Ni_2TiO_2(CO)_2^-$ is obviously split into three peaks located at 2.44 ± 0.05, 2.65 ± 0.04 and 2.94 ± 0.03 eV, with a higher intensity in the third peak. The dominant peaks marked with the letter X of all three photoelectron spectra have a maximum band corresponding to the vertical detachment energy (VDE) values. The VDE values of the ground states for the $Ni_2TiO_2(CO)_n^-$ (n = 2–4) complexes were directly determined to be 2.44 ± 0.05 eV, 2.76 ± 0.04 eV, and 2.86 ± 0.03 eV, respectively. The bands from the spectra without vibrational features prevent us from directly measuring the ground-state ADEs, which can be alternatively estimated by the intersection of a line drawn along the rising edge of the main band with the binding energy axis. The ADE values of the ground states for the $Ni_2TiO_2(CO)_n^-$ (n = 2–4) complexes were evaluated to be 2.17 ± 0.07 eV, 2.43 ± 0.05 eV, and 2.60 ± 0.05 eV, respectively. With the increasing of cluster size, the VDE and ADE values increase, revealing that the electron is stabilized upon the bonding of CO

molecules. Meanwhile, several peaks corresponding to the binding energies of non-highest occupied electron in the spectra could be distinguished, such as the major peaks centered at 2.65 ± 0.04, 2.94 ± 0.03 eV for $Ni_2TiO_2(CO)_2^-$ and at 2.86 ± 0.03, 3.02 ± 0.02 eV for $Ni_2TiO_2(CO)_3^-$.

3.2. Comparison between experimental and theoretical results

We use *ab initio* simulations to gain a clear insight into the geometric and electronic properties of $Ni_2TiO_2(CO)_n^-$ (n = 2–4) clusters by comparing with the results of experiment. The structures, symmetries, and relative energies of the three lowest-energy structures for each size of $Ni_2TiO_2(CO)_n^-$ (n = 2–4) clusters obtained from *ab initio* calculations are given in Fig. 2. The other isomers with higher energies of $Ni_2TiO_2(CO)_n^-$ (n = 3, 4) clusters are listed in Fig. S1 of the ESI.† The lowest-energy structures are designated as *na*, and the metastable structures are designated as *nb*, *nc*, and so on. In all the structures, the three transition metal atoms (one Ti atom and two Ni atoms) form a quasi-line or triangular structure. The two oxygen atoms bond to the Ti atom to form a stoichiometric TiO_2 core, which is different from the results of $NbNiO(CO)_{5-8}^-$ and $TaNiO(CO)_{4-8}^-$ with the competitive binding with oxygen atom to the transition metal centers.[35,36] The oxidation of CO is not favored due to the strong interaction between Ti and O atoms. Unlike $NbNiO(CO)_{7-8}^-$ or $TaNiO(CO)_8^-$,[35,36] the oxidation of CO in $Ni_2TiO_2(CO)_n^-$ (n = 2–4) clusters only occurs in some higher-energy structures such as **3*e***, **3*f***, **3*g***, **4*i***, **4*j***, and **4*k*** with one of the oxygen atoms on Ti binding to the C. The comparison between the experimental photoelectron spectra of $Ni_2TiO_2(CO)_n^-$ (n = 2–4) clusters recorded at 355 nm photons and the BP86 ones of the three lower-energy structures for each size are shown in Fig. 3–5. Table 1 lists the experimental and theoretical VDE and ADE values as well as the theoretical relative energies of the three lower-energy structures for each size of $Ni_2TiO_2(CO)_n^-$ (n = 2–4) clusters. The experimental and theoretical VDE and ADE values as well as the theoretical relative energies of the higher energy structures of $Ni_2TiO_2(CO)_n^-$ (n = 3, 4) clusters are given in Table S3 of the ESI.†

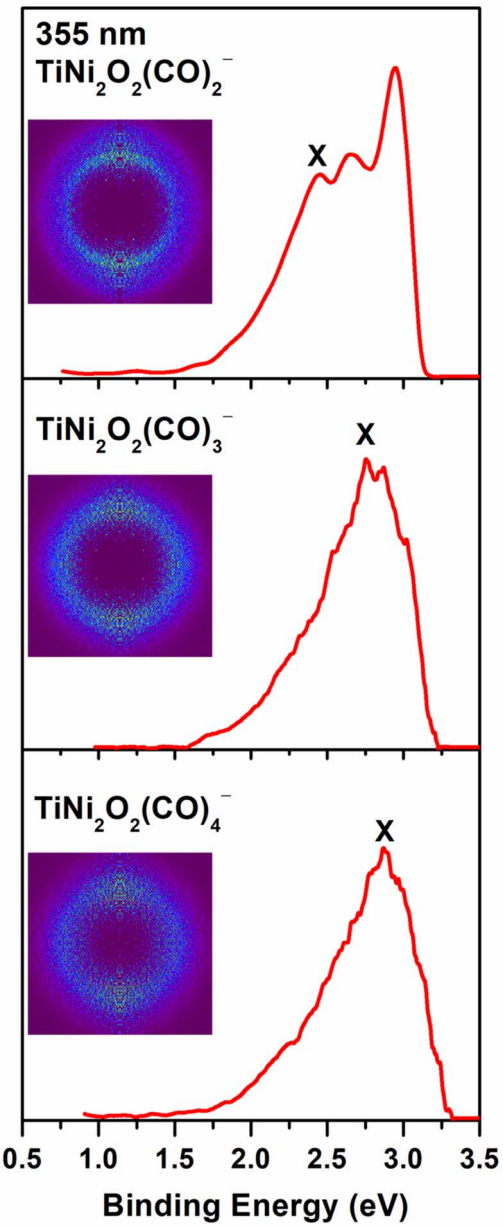

Fig. 1 Photoelectron images of $Ni_2TiO_2(CO)_n^-$ (n = 2–4) at 355 nm. Photoelectron images after inverse Abel transformation are embedded in the photoelectron spectra.

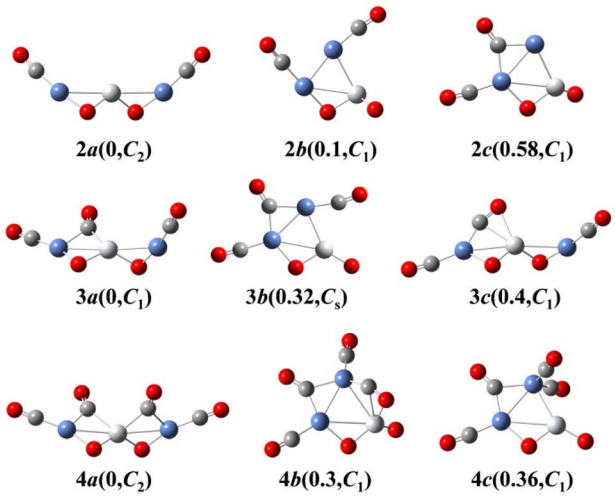

Fig. 2 Schematic diagrams of the three lowest-energy structures for each size of $Ni_2TiO_2(CO)_n^-$ (n = 2–4) clusters (Ti, white; Ni, blue; C, gray; O, red). The relative energy (in units of eV) and symmetry of each cluster are in parentheses.

3.2.1. $Ni_2TiO_2(CO)_2^-$. For n = 2, all the CO molecules bond to Ni atoms. In the lowest-energy structure **2*a***, which has C_2 symmetry, Ni–Ti–Ni is a quasi-line with the angle of Ni–Ti–Ni is 178.01°. The two oxygen atoms are both bridging states between Ti and Ni. The two CO molecules are terminal ones, which is different from the $VNi(CO)_2^-$ (ref. 59) with the involvement of one bridging carbonyl and one terminal carbonyl. The second

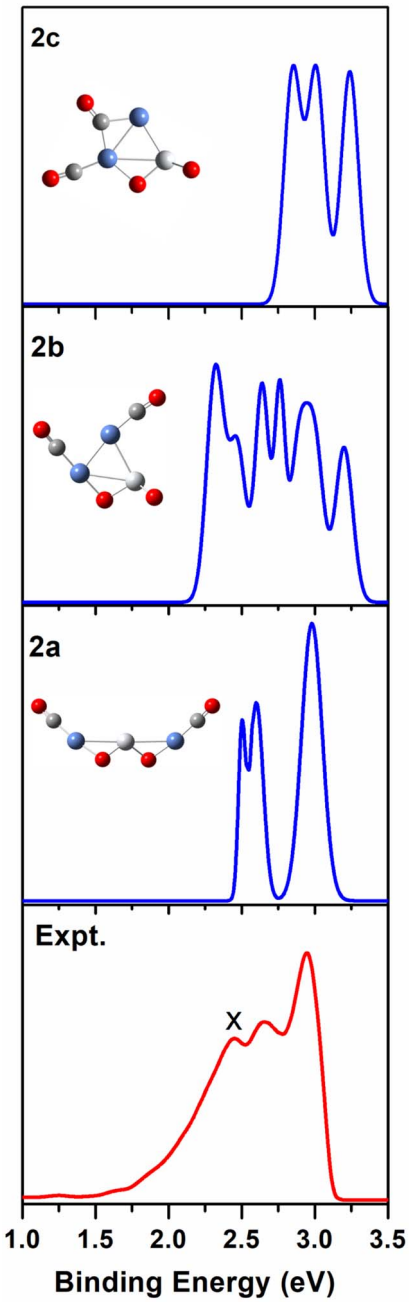

Fig. 3 Comparison between the simulated photoelectron spectra of the three $Ni_2TiO_2(CO)_2^-$ isomers **2*a***, **2*b***, **2*c*** (blue line) and the experimental one at 355 nm (red line).

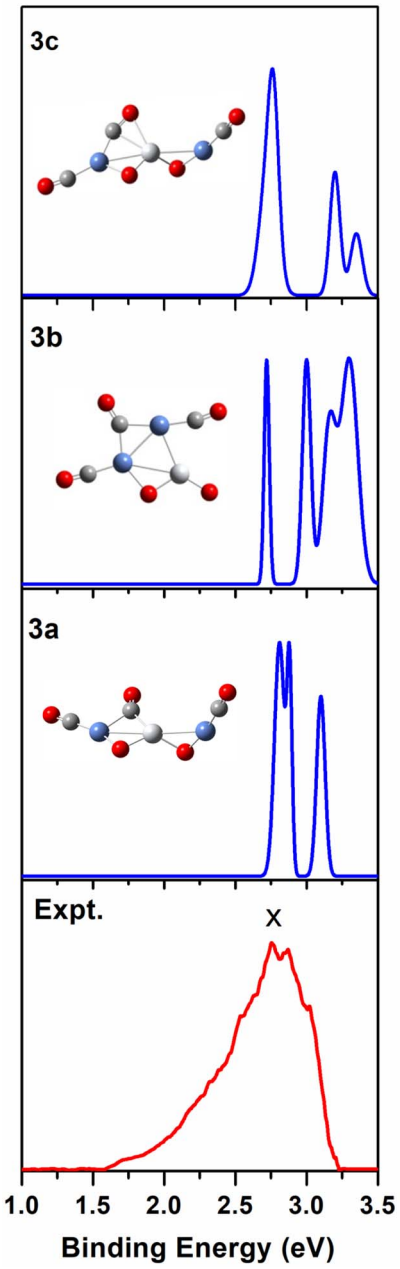

Fig. 4 Comparison between the simulated photoelectron spectra of the three $Ni_2TiO_2(CO)_3^-$ isomers **3*a***, **3*b***, 3*c* (blue line) and the experimental one at 355 nm (red line).

stable structure **2*b*** is only 0.1 eV higher in energy than **2*a***. In **2*b***, the Ti atom and two Ni atoms have a triangular structure. One oxygen atom forms a bridging state between Ti and Ni and another forms a terminal state. The two CO molecules are also terminal ones. In **2*c***, which is similar to **2*b***, One CO molecule forms a bridging state and another forms a terminal state.

As shown in Table 1, the calculated VDEs of both **2*a*** (2.52 eV) and **2*b*** (2.32 eV) are in reasonable agreement with the experimental one (2.44 ± 0.05 eV). The ADEs of both **2*a*** (2.27 eV) and **2*b*** (2.13 eV) are consistent with the experimental result (2.17 ± 0.07 eV). The simulated VDE of **2*c*** is 2.85 eV, which is larger than the experimental result (2.44 ± 0.05 eV). While the ADE of **2*c*** (1.81 eV) is smaller than the experimental one (2.17 ± 0.07 eV). In Fig. 3, the simulated spectrum of **2*a*** has three discrete peaks at 2.52, 2.60, and 2.95 eV, what agrees very well with the experimental photoelectron spectrum (2.44 ± 0.05, 2.65 ± 0.04, 2.94 ± 0.04 eV). The peaks in the simulated spectrum of **2*b*** are apparently more than the experimental result, leading to the conclusion that **2*b*** should be excluded. Therefore, **2*a*** cluster exists in the cluster beam in the experiment.

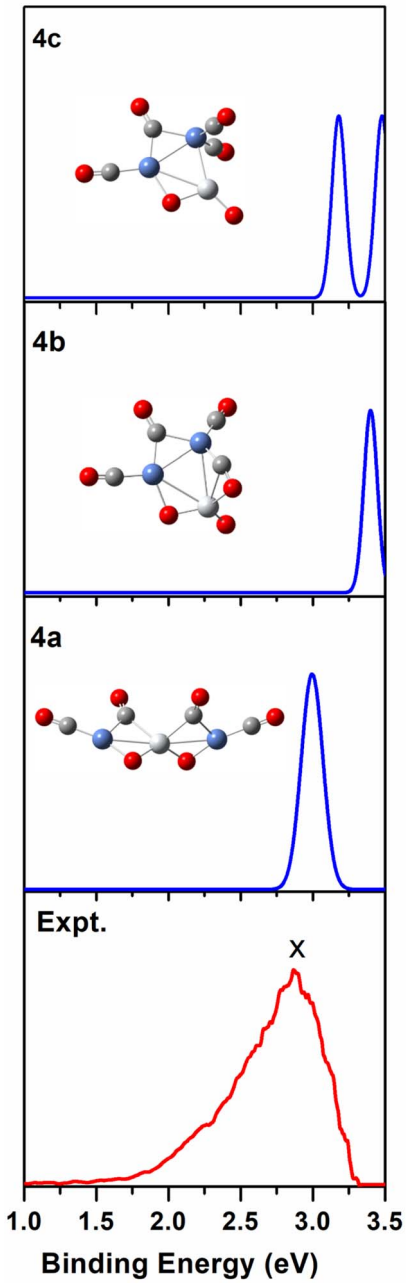

Fig. 5 Comparison between the simulated photoelectron spectra of the three $Ni_2TiO_2(CO)_4^-$ isomers **4*a***, **4*b***, **4*c*** (blue line) and the experimental one at 355 nm (red line).

3.2.2. $Ni_2TiO_2(CO)_3^-$. In all the isomers of $Ni_2TiO_2(CO)_3^-$ clusters, most of the CO molecules adsorb to Ni atoms to form a terminal state or a bridging state between Ti and Ni or between two Ni atoms. The isomers with CO molecule bonding to Ti, such as **3d–3g**, have higher energies. The ground state structure **3*a*** with one bridging carbonyl and two terminal carbonyls is similar to **2*a***. The angle of Ni–Ti–Ni in **3*a*** is 175.60°. It is different from the ground state of $TiNi(CO)_3^-$ with three different types of CO bonds[9] due to the discrepancy between the number of Ni atoms and the presence of oxygen.

Table 1 Experimental and theoretical vertical detachment energies (VDEs) and adiabatic detachment energies (ADEs) as well as theoretical relative energies (ΔE) of the three lowest-energy structures for each size of $Ni_2TiO_2(CO)_n^-$ ($n = 2$–4) clusters

			VDE (eV)		ADE (eV)	
n	Isomers	ΔE (eV)	Theo.	Exp.	Theo.	Exp.
2	**2*a***	0.00	2.52	2.44(5)	2.27	2.17(7)
	2*b*	0.10	2.32		2.13	
	2*c*	0.58	2.85		1.81	
3	**3*a***	0.00	2.81	2.76(4)	2.54	2.43(5)
	3*b*	0.32	2.71		2.38	
	3*c*	0.40	2.73		2.40	
4	**4*a***	0.00	2.98	2.86(3)	2.72	2.60(5)
	4*b*	0.30	3.40		2.89	
	4*c*	0.36	3.18		2.86	

Table 2 The average bond lengths (in units of Å) and bond angles (in units of °) of the lowest-energy structures of $Ni_2TiO_2(CO)_n^-$ ($n = 2$–4) clusters

n	2	3	4
Ti–O	1.760	1.778	1.78
Ni–C	1.694	1.79	1.835
Ti–Ni	2.648	2.628	2.654
Ni–O	1.822	1.83	1.84
∠Ni–Ti–Ni	178.01	175.6	171.1

The meta-stable structure **3*b***, in which the three metal atoms have triangle configuration, is 0.32 eV higher in energy than **3*a***. The **3*c*** isomer is 0.4 eV higher in energy than **3*a*** though it has similar configuration to **3*a*** with the bridging carbonyl being side-on-bonded instead.

According to Table 1 and S3 of the ESI,† among the seven $Ni_2TiO_2(CO)_3^-$ isomers, **3*a***, **3*b***, and **3*c*** have both comparable VDE and ADE values to experimental ones. From Fig. 4 we can see that there are three peaks at 2.81, 2.88, and 3.1 eV in the simulated PES of **3*a***, which coincides with the experimental values (2.76 ± 0.04, 2.86 ± 0.03, 3.02 ± 0.02 eV) well. However, the number of the peaks (four peaks centered at 2.71, 3, 3.16, and 3.3 eV) in the simulated PES of **3*b*** is larger than that in experiment. For **3*c***, except for the first peak at 2.73 eV in the simulated PES is comparable to the experimental result of 2.76 eV, the other two peaks at 3.19 and 3.32 eV cannot match the experimental values of 2.86 ± 0.03 and 3.02 ± 0.02 eV, respectively. This suggests that the **3*a*** isomer should be responsible for the $n = 3$ spectrum.

3.2.3. $Ni_2TiO_2(CO)_4^-$. With the increase in cluster size, the potential energy surface becomes more complicated and the number of isomers increases. There are 11 isomers for $Ni_2TiO_2(CO)_4^-$ clusters. Most of the CO molecules adsorb to Ni atoms to form a terminal state or a bridging state between Ti and Ni or between two Ni atoms. The ground state structure **4*a*** with C_2 symmetry is similar to **2*a*** and **3*a***. The angle of Ni–Ti–Ni in **4*a*** is 171.10°. Though it is different from the lowest-energy structure of $TiNi(CO)_4^-$ cluster with three bridging carbonyls

Table 3 The natural electron configuration of the lowest-energy structures of $Ni_2TiO_2(CO)_n^-$ (n = 2–4) clusters

		Natural electron configuration		
		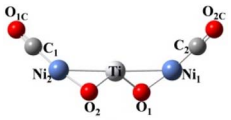	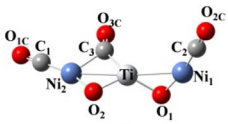	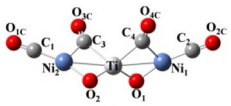
	Valence electron	**2*a***	**3*a***	**4*a***
Ti	$3d^2 4s^2$	$4s^{0.4}3d^{2.3}4p^{0.3}$	$4s^{0.2}3d^{2.6}4p^{0.4}4d^{0.1}$	$4s^{0.2}3d^{2.8}4p^{0.5}4d^{0.1}$
Ni_1	$3d^8 4s^2$	$4s^{0.6}3d^{9.1}4p^{0.3}$	$4s^{0.6}3d^{9.1}4p^{0.2}$	$4s^{0.5}3d^{9}4p^{0.5}$
Ni_2	$3d^8 4s^2$	$4s^{0.6}3d^{9.1}4p^{0.3}$	$4s^{0.5}3d^{9}4p^{0.5}$	$4s^{0.5}3d^{9}\ 4p^{0.5}$
O_1	$2s^2 2p^4$	$2s^{1.8}2p^5$	$2s^{1.8}2p^{5.}$	$2s^{1.8}2p^5$
O_2	$2s^2 2p^4$	$2s^{1.8}2p^5$	$2s^{1.8}2p^5$	$2s^{1.8}2p^5$
C_1	$2s^2 2p^2$	$2s^{1.3}2p^{2.2}$	$2s^{1.3}2p^{2.2}$	$2s^{1.3}2p^{2.2}$
O_{1C}	$2s^2 2p^4$	$2s^{1.7}2p^{4.8}$	$2s^{1.7}2p^{4.7}$	$2s^{1.7}2p^{4.7}$
C_2	$2s^2 2p^2$	$2s^{1.3}2p^{2.2}$	$2s^{1.3}2p^{2.3}$	$2s^{1.3}2p^{2.2}$
O_{2C}	$2s^2 2p^4$	$2s^{1.7}2p^{4.8}$	$2s^{1.7}2p^{4.8}$	$2s^{1.7}2p^{4.7}$
C_3	$2s^2 2p^2$	—	$2s^{1.2}2p^{2.4}$	$2s^{1.2}2p^{2.4}$
O_{3C}	$2s^2 2p^4$	—	$2s^{1.7}2p^{4.7}$	$2s^{1.7}2p^{4.7}$
C_4	$2s^2 2p^2$	—	—	$2s^{1.2}2p^{2.4}$
O_{4C}	$2s^2 2p^4$	—	—	$2s^{1.7}2p^{4.7}$

and one terminal carbonyl,[9] the terminal carbonyls only bond to Ni for both of them. Except for **4*a***, **4*f***, and **4*j***, the Ti atom and two Ni atoms form a triangular structure in $Ni_2TiO_2(CO)_4^-$ clusters.

It can be seen from Tables 1 and S3 of the ESI† that the VDE (2.98 eV) and ADE (2.72 eV) of **4*a*** match the experimental VDE 2.86 ± 0.03 eV and ADE 2.60 ± 0.05 eV well, respectively. The VDEs of the meta-stable structures of $Ni_2TiO_2(CO)_4^-$ clusters are larger than the experimental ones. In Fig. 5, there is only one main peak at 2.98 eV in the simulated PES of **4*a***, which is identical to the experimental feature. The peak position in the simulated spectrum of **4*b*** deviated from the experimental one. Meanwhile, the peaks in the simulated spectrum of **4*c*** are more than the experimental result. Therefore, **4*a*** is the most probable structure detected in experiment.

3.3. Geometric and electronic properties of the lowest-energy structures

The above-mentioned comparison between experimental and theoretical results reveals that the lowest-energy structures of $Ni_2TiO_2(CO)_n^-$ (n = 2–4) clusters are the ones with the three transition metal atoms forming a quasi-line. **2*a*** has C_2 symmetry. The two CO molecules added to the two Ni atoms form terminal ones. **3*a*** is a structure with the third CO molecule located in the middle of Ti and Ni forming bridge coordination. The fourth CO molecule in **4*a*** locates at the middle of Ti and Ni on the other side and **4*a*** also has C_2 symmetry. Table 2 lists several characteristic bond lengths and bond angles of the ground state structures of $Ni_2TiO_2(CO)_n^-$ (n = 2–4) clusters. The average bond lengths of Ti–O, Ti–Ni, Ni–O, and the distance between Ni and Ni (5.295, 5.252, and 5.292 Å for **2*a***, **3*a***, and **4*a***, respectively) remain constant as the cluster size increases, meaning that the framework of Ni_2TiO_2 is stable in the lowest-energy structure of $Ni_2TiO_2(CO)_n^-$ (n = 2–4) clusters. The average distances between Ni and C become longer as the cluster size increases. The angle of Ni–Ti–Ni decreases as the cluster size increasing. Thus, the interaction between Ni and C becomes weaker with the cluster size increasing.

The natural electron configuration of the lowest-energy structures of $Ni_2TiO_2(CO)_n^-$ (n = 2–4) clusters is shown in Table 3. The valence electron configuration of the element Ti is $3d^2 4s^2$, while its 4s orbital lose electrons as well as 3d, 4p and 4d orbitals gain extra electrons in the lowest-energy structures of $Ni_2TiO_2(CO)_n^-$ (n = 2–4) clusters. The Ti atom in **2*a***, **3*a***, and **4*a*** totally loses 1, 0.7, and 0.4 electrons, respectively. In the two Ni atoms of all the ground state structures, though the 4s orbital lose electrons and 3d and 4p orbitals gain extra electrons, the total electrons remain unchanged. The two O atoms bonded to Ti totally gain 1.6 electrons since the 2s orbital loses 0.2 electrons and the 2p orbital gains 1 electron for each O atom. The number of electrons gained by the oxygen atom is almost equal to the number of electrons lost by the C atom in one CO molecule. Thus, the CO molecules do not gain or lose electrons. In conclusion, the extra electron is enriched on O atoms attached to Ti. The Ti atom loses electrons and the O atoms attached to Ti gain electrons, indicating strong interaction between Ti and O. Meanwhile, the interaction between CO molecules and Ni_2TiO_2 unit is weak. All those lead to no CO oxidation in the lowest-energy structures of $Ni_2TiO_2(CO)_n^-$ (n = 2–4) clusters.

4. Conclusion

By combining photoelectron imaging spectroscopy and *ab initio* calculations, the low-lying isomers, structural evolution, relative stabilities, and electronic structures of $Ni_2TiO_2(CO)_n^-$ (n = 2–4) clusters are investigated. The VDEs and ADEs become larger with the increase in cluster size, meaning that the binding of

electrons is stronger as the cluster size increasing. In the lowest-energy structures of $Ni_2TiO_2(CO)_n^-$ ($n = 2$–4) clusters, the three transition metal atoms (one Ti atom and two Ni atoms) form a quasi-line, which is different from triangular structure for trimetallic active center. It provides more evidence for the reaction of multicomponent alloy with CO. The adding of CO molecules makes the interaction between Ni and C weaker. The natural electron configuration shows that the strong interaction between O and Ti and the weak interaction between CO molecules and Ni_2TiO_2 unit lead to the absence of CO oxidation. Our results provide new light on the geometric and electronic structures of nickel–titanium dioxide carbonyl anions and will have important implications on the CO adsorbed on the surfaces/interfaces of alloy.

Conflicts of interest

There are no conflicts of interest to declare.

Acknowledgements

This work was supported by the National Natural Science Foundation of China (No. 21976049, 12004094, 12004095, 11904251), the Natural Science Foundation of Hebei Province (No. B2021402006, F2019402063), the Scientific and Technological Research in Higher Education Institutions of Hebei Province (No. BJK2022057, BJK2023041), and the Handan Science and Technology Bureau (No. 21422901248).

References

1 Y. Ishii and M. Tsutsui, Organotransition-Metal Chemistry, *Science*, 1975, **188**, 1224–1225.
2 B. Yoon, H. Häkkinen, U. Landman, *et al.*, Charging Effects on Bonding and Catalyzed Oxidation of CO on Au_8 Clusters on MgO, *Science*, 2005, **307**, 403–407.
3 D. K. Böhme and H. Schwarz, Gas-Phase Catalysis by Atomic and Cluster Metal Ions: The Ultimate Single-Site Catalysts, *Angew. Chem., Int. Ed.*, 2005, **44**, 2336–2354.
4 H.-J. Freund, G. Meijer, M. Scheffler, *et al.*, CO Oxidation as a Prototypical Reaction for Heterogeneous Processes, *Angew. Chem., Int. Ed.*, 2011, **50**, 10064–10094.
5 M. Zhou, L. Andrews and C. W. Bauschlicher, Spectroscopic and Theoretical Investigations of Vibrational Frequencies in Binary Unsaturated Transition-Metal Carbonyl Cations, Neutrals, and Anions, *Chem. Rev.*, 2001, **101**, 1931–1962.
6 A. Fielicke, P. Gruene, G. Meijer, *et al.*, The adsorption of CO on transition metal clusters: A case study of cluster surface chemistry, *Surf. Sci.*, 2009, **603**, 1427–1433.
7 H. Schwarz and K. R. Asmis, Identification of Active Sites and Structural Characterization of Reactive Ionic Intermediates by Cryogenic Ion Trap Vibrational Spectroscopy, *Chem.–Eur. J.*, 2019, **25**, 2112–2126.
8 J.-B. Ma, Z.-C. Wang, M. Schlangen, *et al.*, On the Origin of the Surprisingly Sluggish Redox Reaction of the N_2O/CO Couple Mediated by $[Y_2O_2]^+$. and $[YAlO_2]^+$. Cluster Ions in the Gas Phase, *Angew. Chem., Int. Ed.*, 2013, **52**, 1226–1230.
9 J. Zou, H. Xie, Q. Yuan, *et al.*, Probing the bonding of CO to heteronuclear group 4 metal–nickel clusters by photoelectron spectroscopy, *Phys. Chem. Chem. Phys.*, 2017, **19**, 9790–9797.
10 L. Jiang and Q. Xu, Observation of Anomalous C–O Bond Weakening on Discandium and Activation Process to CO Dissociation, *J. Am. Chem. Soc.*, 2005, **127**, 42–43.
11 Q. Xu, L. Jiang and N. Tsumori, *cyclo*-$Ti_3[\eta^2(\mu_2\text{-C,O})]_3$: A Side-on-Bonded Polycarbonyl Titanium Cluster with Potentially Antiaromatic Character, *Angew. Chem., Int. Ed.*, 2005, **44**, 4338–4342.
12 A. M. Ricks, Z. E. Reed and M. A. Duncan, Infrared spectroscopy of mass-selected metal carbonyl cations, *J. Mol. Spectrosc.*, 2011, **266**, 63–74.
13 A. D. Brathwaite, J. A. Maner and M. A. Duncan, Testing the Limits of the 18-Electron Rule: The Gas-Phase Carbonyls of Sc^+ and Y^+, *Inorg. Chem.*, 2014, **53**, 1166–1169.
14 H. Xie, J. Wang, Z. Qin, *et al.*, Octacoordinate Metal Carbonyls of Lanthanum and Cerium: Experimental Observation and Theoretical Calculation, *J. Phys. Chem. A*, 2014, **118**, 9380–9385.
15 J. Jin, T. Yang, K. Xin, *et al.*, Octacarbonyl Anion Complexes of Group Three Transition Metals $[TM(CO)_8]^-$ (TM = Sc, Y, La) and the 18-Electron Rule, *Angew. Chem., Int. Ed.*, 2018, **57**, 6236–6241.
16 J. Jin, S. Pan, X. Jin, *et al.*, Octacarbonyl Anion Complexes of the Late Lanthanides $Ln(CO)_8^-$ (Ln = Tm, Yb, Lu) and the 32-Electron Rule, *Chem.–Eur. J.*, 2019, **25**, 3229–3234.
17 D. T. Moore, J. Oomens, J. R. Eyler, *et al.*, Gas-Phase IR Spectroscopy of Anionic Iron Carbonyl Clusters, *J. Am. Chem. Soc.*, 2004, **126**, 14726–14727.
18 H.-J. Zhai, B. Kiran, B. Dai, *et al.*, Unique CO Chemisorption Properties of Gold Hexamer: $Au_6(CO)_n^-$ ($n = 0$–3), *J. Am. Chem. Soc.*, 2005, **127**, 12098–12106.
19 I. Swart, F. M. F. de Groot, B. M. Weckhuysen, *et al.*, The Effect of Charge on CO Binding in Rhodium Carbonyls: From Bridging to Terminal CO, *J. Am. Chem. Soc.*, 2008, **130**, 2126–2127.
20 C. Chi, J. Cui, Z. H. Li, *et al.*, Infrared photodissociation spectra of mass selected homoleptic dinuclear iron carbonyl cluster anions in the gas phase, *Chem. Sci.*, 2012, **3**, 1698–1706.
21 G. Wang, J. Cui, C. Chi, *et al.*, Bonding in homoleptic iron carbonyl cluster cations: a combined infrared photodissociation spectroscopic and theoretical study, *Chem. Sci.*, 2012, **3**, 3272–3279.
22 X. Zhou, J. Cui, Z. H. Li, *et al.*, Infrared Photodissociation Spectroscopic and Theoretical Study of Homoleptic Dinuclear Chromium Carbonyl Cluster Cations with a Linear Bridging Carbonyl Group, *J. Phys. Chem. A*, 2012, **116**, 12349–12356.
23 J. Cui, X. Zhou, G. Wang, *et al.*, Infrared Photodissociation Spectroscopy of Mass Selected Homoleptic Copper Carbonyl Cluster Cations in the Gas Phase, *J. Phys. Chem. A*, 2013, **117**, 7810–7817.
24 J. Cui, X. Zhou, G. Wang, *et al.*, Infrared Photodissociation Spectroscopy of Mass-Selected Homoleptic Cobalt Carbonyl

Cluster Cations in the Gas Phase, *J. Phys. Chem. A*, 2014, **118**, 2719–2727.

25 J. Zou, H. Xie, D. Dai, *et al.*, Sequential bonding of CO molecules to a titanium dimer: A photoelectron velocity-map imaging spectroscopic and theoretical study of $Ti2(CO)_n^-$ (n = 1–9), *J. Chem. Phys.*, 2016, **145**, 184302.

26 N. Zhang, M. Luo, C. Chi, *et al.*, Infrared Photodissociation Spectroscopy of Mass-Selected Heteronuclear Iron–Copper Carbonyl Cluster Anions in the Gas Phase, *J. Phys. Chem. A*, 2015, **119**, 4142–4150.

27 Z. Liu, J. Zou, Z. Qin, *et al.*, Photoelectron Velocity Map Imaging Spectroscopy of Lead Tetracarbonyl–Iron Anion $PbFe(CO)_4^-$, *J. Phys. Chem. A*, 2016, **120**, 3533–3538.

28 Z. Jumei, Z. Liu, G. Li, *et al.*, CO activation by the heterobinuclear transition metal-iron clusters: A photoelectron spectroscopic and theoretical study, *J. Energy Chem.*, 2021, **63**, 344–350.

29 H. Qu, F. Kong, G. Wang, *et al.*, Infrared Photodissociation Spectroscopic and Theoretical Study of Heteronuclear Transition Metal Carbonyl Cluster Cations in the Gas Phase, *J. Phys. Chem. A*, 2016, **120**, 7287–7293.

30 Z. Liu, H. Xie, Z. Qin, *et al.*, Structural Evolution of Homoleptic Heterodinuclear Copper–Nickel Carbonyl Anions Revealed Using Photoelectron Velocity-Map Imaging, *Inorg. Chem.*, 2014, **53**, 10909–10916.

31 H. Xie, Z. Liu, X. Xing, *et al.*, Infrared photodissociation spectroscopy of $MO(CO)_5^+$ (M = Sc, Y, La and Ce) in the gas phase, *Chem. Phys. Lett.*, 2015, **628**, 66–70.

32 H. Xie, Z. Liu, Z. Zhao, *et al.*, Observing the Transition from Equatorial to Axial CO Chemisorption: Infrared Photodissociation Spectroscopy of Yttrium Oxide–Carbonyls, *Inorg. Chem.*, 2016, **55**, 5502–5506.

33 Y. Chen, K. Xin, J. Jin, *et al.*, Infrared photodissociation spectroscopic investigation of $TMO(CO)_n^+$ (TM = Sc, Y, La): testing the 18-electron rule, *Phys. Chem. Chem. Phys.*, 2019, **21**, 6743–6749.

34 Z. Liu, L. Hou, Y. Li, *et al.*, Thermodynamics and Kinetics of Gas-Phase CO Oxidation on the Scandium Monoxide Carbonyl Complexes, *J. Phys. Chem. A*, 2020, **124**, 924–931.

35 J. Zhang, Y. Li, Z. Liu, *et al.*, Ligand-Mediated Reactivity in CO Oxidation of Niobium–Nickel Monoxide Carbonyl Complexes: The Crucial Roles of the Multiple Adsorption of CO Molecules, *J. Phys. Chem. Lett.*, 2019, **10**, 1566–1573.

36 J. Zhang, Y. Li, Y. Bai, *et al.*, CO oxidation on the heterodinuclear tantalum–nickel monoxide carbonyl complex anions, *Chin. Chem. Lett.*, 2021, **32**, 854–860.

37 M. Haruta, S. Tsubota, T. Kobayashi, *et al.*, Low-Temperature Oxidation of CO over Gold Supported on TiO_2, α-Fe_2O_3, and Co_3O_4, *J. Catal.*, 1993, **144**, 175–192.

38 X. Xie, Y. Li, Z.-Q. Liu, *et al.*, Low-temperature oxidation of CO catalysed by Co_3O_4 nanorods, *Nature*, 2009, **458**, 746–749.

39 B. Xu, Y.-X. Zhao, X.-L. Ding, *et al.*, Reactions of $Sc_2O_4^-$ and $La_2O_4^-$ Clusters with CO: A comparative study, *Int. J. Mass Spectrom.*, 2013, **334**, 1–7.

40 C. Chi, H. Qu, L. Meng, *et al.*, CO Oxidation by Group 3 Metal Monoxide Cations Supported on $[Fe(CO)_4]^{2-}$, *Angew. Chem., Int. Ed.*, 2017, **56**, 14096–14101.

41 L.-N. Wang, X.-N. Li and S.-G. He, Catalytic CO Oxidation by Noble-Metal-Free $Ni_2VO_{4,5}^-$ Clusters: A CO Self-Promoted Mechanism, *J. Phys. Chem. Lett.*, 2019, **10**, 1133–1138.

42 Z. Qin, X. Wu and Z. Tang, Note: A novel dual-channel time-of-flight mass spectrometer for photoelectron imaging spectroscopy, *Rev. Sci. Instrum.*, 2013, **84**, 066108.

43 Y. Gao, W. Huang, J. Woodford, *et al.*, Detecting Weak Interactions between Au^- and Gas Molecules: A Photoelectron Spectroscopic and *ab Initio* Study, *J. Am. Chem. Soc.*, 2009, **131**, 9484–9485.

44 W. Huang, H.-J. Zhai and L.-S. Wang, Probing the Interactions of O_2 with Small Gold Cluster Anions (Au_n^-, n = 1–7): Chemisorption *vs.* Physisorption, *J. Am. Chem. Soc.*, 2010, **132**, 4344–4351.

45 Z. Qin, R. Cong, X. Wu, *et al.*, Photoelectron velocity-map imaging spectroscopic and theoretical study on the reactivity of the gold atom toward CH_3SH, CH_3OH, and H_2O, *J. Chem. Phys.*, 2013, **139**, 034315.

46 V. Jonas and W. Thiel, Theoretical study of the vibrational spectra of the transition metal carbonyls $M(CO)_6$ [M = Cr, Mo, W], $M(CO)_5$ [M = Fe, Ru, Os], and $M(CO)_4$ [M = Ni, Pd, Pt], *J. Chem. Phys.*, 1995, **102**, 8474–8484.

47 A. D. Becke, Density-functional exchange-energy approximation with correct asymptotic behavior, *Phys. Rev. A*, 1988, **38**, 3098–3100.

48 J. P. Perdew, Density-functional approximation for the correlation energy of the inhomogeneous electron gas, *Phys. Rev. B: Condens. Matter Mater. Phys.*, 1986, **33**, 8822–8824.

49 F. Weigend and R. Ahlrichs, Balanced basis sets of split valence, triple zeta valence and quadruple zeta valence quality for H to Rn: Design and assessment of accuracy, *Phys. Chem. Chem. Phys.*, 2005, **7**, 3297–3305.

50 J. Zheng, X. Xu and D. G. Truhlar, Minimally augmented Karlsruhe basis sets, *Theor. Chem. Acc.*, 2011, **128**, 295–305.

51 E. Papajak, J. Zheng, X. Xu, *et al.*, Perspectives on Basis Sets Beautiful: Seasonal Plantings of Diffuse Basis Functions, *J. Chem. Theory Comput.*, 2011, **7**, 3027–3034.

52 J. Akola, M. Manninen, H. Häkkinen, *et al.*, Photoelectron spectra of aluminum cluster anions: Temperature effects and *ab initio* simulations, *Phys. Rev. B: Condens. Matter Mater. Phys.*, 1999, **60**, R11297–R11300.

53 W.-J. Chen, H.-J. Zhai, X. Huang, *et al.*, On the electronic structure of mono-rhenium oxide clusters: ReO_n^- and ReO_n (n = 3,4), *Chem. Phys. Lett.*, 2011, **512**, 49–53.

54 H.-J. Zhai, X.-H. Zhang, W.-J. Chen, *et al.*, Stoichiometric and Oxygen-Rich $M_2O_n^-$ and M_2O_n (M = Nb, Ta; n = 5–7) Clusters: Molecular Models for Oxygen Radicals, Diradicals, and Superoxides, *J. Am. Chem. Soc.*, 2011, **133**, 3085–3094.

55 H.-J. Zhai, W.-J. Chen, X. Huang, *et al.*, On the electronic structure and conflicting d-orbital aromaticity in the $Re_3O_3^-$ cluster, *RSC Adv.*, 2012, **2**, 2707–2712.

56 D. J. Tozer and N. C. Handy, Improving virtual Kohn–Sham orbitals and eigenvalues: Application to excitation energies and static polarizabilities, *J. Chem. Phys.*, 1998, **109**, 10180–10189.

57 J. Akola, M. Manninen, H. Häkkinen, *et al.*, Aluminum cluster anions: Photoelectron spectroscopy and *ab initio* simulations, *Phys. Rev. B: Condens. Matter Mater. Phys.*, 2000, **62**, 13216–13228.

58 M. Frisch, G. Trucks, H. Schlegel, *et al.*, *Gaussian 09, Revision-D.01*, Gaussian, Inc., Wallingford CT, 2013.

59 Q. Yuan, Z. Jumei, Z. Jinghan, *et al.*, Photoelectron velocity map imaging spectroscopic and theoretical study of heteronuclear vanadium-nickel carbonyl anions $VNi(CO)_n^-$ $(n = 2–6)$, *J. Chem. Phys.*, 2018, **149**, 144305.